Differential Metabolic Activity in the Striosome and Matrix Compartments of the Rat Striatum during Natural Behaviors

Lucy L. Brown,[1] Samuel M. Feldman,[2] Diane M. Smith,[1] James R. Cavanaugh,[2] Robert F. Ackermann,[3] and Ann M. Graybiel[4]

[1]Departments of Neurology and Neuroscience, Albert Einstein College of Medicine, Bronx, New York 10461, [2]Center for Neural Science, New York University, New York, New York 10003, [3]Department of Psychiatry and Behavioral Neurobiology, University of Alabama School of Medicine, Birmingham, Alabama 35294, and [4]Department of Brain and Cognitive Sciences and the McGovern Institute for Brain Research, Massachusetts Institute of Technology, Cambridge, Massachusetts 02139

The striosome and matrix compartments of the striatum are clearly identified by their neurochemical expression patterns and anatomical connections. To determine whether these compartments are distinguishable functionally, we used [^{14}C]deoxyglucose metabolic mapping in the rat and tested whether neutral behavioral states (free movement, gentle restraint, and focal tactile stimulation under gentle restraint) were associated with regions of high metabolic activity in the matrix, in striosomes, or in both. We identified metabolic peaks in the striatum by means of image analysis, striosome–matrix boundaries by [^{3}H]naloxone binding, and primary somatosensory corticostriatal input clusters by injections of anterograde tracer into electrophysiologically identified sites in SI. Peak metabolic activity was primarily confined to the matrix compartment under each behavioral condition. These findings show that during relatively neutral behavioral conditions the balance of activity between the two compartments favors the matrix and suggest that this balance is present in the striatum as part of normal behavior and processing of afferent activity.

Key words: basal ganglia; caudate-putamen; deoxyglucose; metabolic mapping; somatosensory cortex; striosome; matrix

The striatum is characterized by a striking anatomical architecture that divides it into striosomes and matrix (Graybiel and Ragsdale, 1978; Graybiel, 1990; Gerfen, 1992). These compartments exhibit different levels of expression of neurotransmitter-related molecules ranging from receptors to second messengers. They also have different input–output connections and different complements of striatal interneurons (Donoghue and Herkenham, 1986; Jimenez-Castellanos and Graybiel, 1987; Gerfen, 1989; Ragsdale and Graybiel, 1990; Kincaid and Wilson, 1996; van Vulpen and van der Kooy, 1998). The large matrix compartment itself has patchy sets of inputs and outputs, suggesting that it, too, is divided into modular domains that have been called matrisomes (Flaherty and Graybiel, 1994; Kincaid and Wilson, 1996). It is still not known, however, how these anatomically identified compartments are related to functional processing in the striatum. For example, despite evidence for heterogeneity in activity patterns of neurons recorded in awake behaving animals (Schultz and Romo, 1988; Alexander and Crutcher, 1990; Kimura, 1990; Carelli and West, 1991; Hikosaka, 1991; Rolls, 1994; Kermadi and Joseph, 1995; Mink, 1996; Trytek et al., 1996; Jog et al., 1999), the sites of recordings have generally not been referable to particular compartments. Clustering of functionally related neurons has been observed in a few studies, suggesting that the anatomical clusters could have functional counterparts (Crutcher and DeLong, 1984; Liles and Updyke, 1985; Carelli and West, 1991; Jog et al., 1999), but differences in the functional properties of nearby units have also been found. Moreover, there is widespread electronic coupling of some striatal interneurons (Koos and Tepper, 1999), suggesting that functional processing may blur anatomical boundaries. Similarly, although most striatal input fibers and output neurons form clusters distinguishable in anatomical labeling studies, even the most vividly patchy anatomical labeling is always accompanied by more diffuse labeling likely representing diffuse projection systems (Jones et al., 1977; Künzle, 1977; Selemon and Goldman-Rakic, 1985; Flaherty and Graybiel, 1991; Giménez-Amaya and Graybiel, 1991; Cowan and Wilson, 1994; Kincaid and Wilson, 1996; Parthasarathy and Graybiel, 1997; Alloway et al., 1999; Wright et al., 1999). Thus neither current electrophysiological evidence nor current anatomical evidence has settled the question of whether compartmentation within the striatum exists at the functional level, or whether the compartments are coactive in the course of natural behaviors.

To address this issue, we used the [14C]deoxyglucose (2DG) mapping method to study metabolic activity in the striatum of awake behaving rats both in the free-moving state and during quiet restraint and gentle tactile stimulation. Although such metabolic activity is an indirect measure of ongoing neural activity (Durham and Woolsey, 1977; Sokoloff et al., 1977; Hubel et al., 1978; Juliano and Whitsel, 1987; Friedman and Goldman-Rakic, 1994), the 2DG method has the high resolution and broad coverage that allowed us to compare tissue activity levels with compartmental distribution patterns determined in the striatum postmortem. Our findings suggest that neural activity predominates in

Received July 5, 2001; revised Oct. 11, 2001; accepted Oct. 12, 2001.

This work was supported by National Institutes of Health Grants NS21356 and NS20253 (L.L.B.) and National Institutes of Health Javits Award NS25529 (A.M.G.). We are grateful to Adam Hartley and H. F. Hall for help with the figures, Patricia Harlan for work with histology, and the Image Analysis and Graphics Core at the Kennedy Center, Albert Einstein College of Medicine.

In memory of Harvey Etra.

Correspondence should be addressed to Dr. Lucy L. Brown, Albert Einstein College of Medicine, 1300 Morris Park Avenue, K-601, Bronx, NY 10461. E-mail: brown@aecom.yu.edu.

the matrix compartment of the striatum under behavioral conditions of rest, free movement, and restraint as well as during specific afferent activation in the form of somatosensory stimulation.

MATERIALS AND METHODS

Somatosensory stimulation and [^{14}C]deoxyglucose autoradiography. Experiments were performed on 25 male Sprague Dawley rats (250–350 gm; Taconic Farms, Germantown, NY) housed on a daylight cycle with *ad libitum* access to food and water. The rats were divided into seven experimental groups. The first, free-movement group ($n = 5$) was made up of rats allowed to move freely in a dark observation chamber or in a laboratory cage containing chocolate squares. Other groups received somatosensory stimulation on the left hindlimb (HL, $n = 3$), left forelimb (FL, $n = 4$), or left vibrissae (VIB, $n = 4$), or served as matched restrained control groups, receiving similar gentle restraint but no stimulation ($n = 3$ for hindlimb; $n = 4$ for forelimb; and $n = 2$ for vibrissa).

All rats were brought from the animal facility to the laboratory in cages the night before experiments were done. Deoxyglucose experiments were performed according to established procedures (Sokoloff et al., 1977; Crane and Porrino, 1989). The morning of the experiment, the rats were anesthetized with halothane; catheters were implanted in the external iliac vein and artery and were externalized at the back of the neck. The rats were returned to their cages to recover for 2–4 hr. Rats in the free-moving group were either left in their cages, to which squares of chocolate were added ($n = 2$), or moved to a 2.5 cubic foot sound-attenuating chamber with ambient white noise ~20 min before injection of deoxyglucose to allow time for exploration ($n = 3$). A 0.5 ml bolus of 2-[1-^{14}C]deoxy-D-glucose (DuPont NEN; Boston, MA) in 0.9% saline was injected through the intravenous catheter at a concentration of 0.05 μCi/gm of body weight. To quantify the glucose utilization rate, 13 arterial samples were taken over the course of the 45 min experimental period (Sokoloff et al., 1977). During the period after injection, the rats sat quietly, groomed, explored, or ate.

All HL and FL rats, whether stimulated or restrained only, were placed in a Plexiglas restrainer (Braintree Scientific, Inc., Braintree, MA) 20 min before 2DG injection, with the hindlimb or forelimb extended and secured with a cuff of soft surgical tape onto the surface of the Plexiglas restrainer. Rats in the VIB groups were placed in a movement-restricting plastic cone with an opening allowing experimenter access to the vibrissae. For the stimulation groups, each rat was stimulated for at least 10 min before injection of the 2DG bolus as above and for 45 min afterward. In the stimulated HL and FL animals, a nylon bristle attached to a rotating wheel was swept across the hairy skin of the dorsal surface of the limb at a rate of three to four sweeps/sec. The bristle bent at a pressure of 2.5 gm and moved over a range of 1–2 cm. The FL stimulus swept between the elbow and the wrist; the HL stimulus traversed a path between the patella and the pelvis. In the VIB group, stimulation was applied to a single vibrissa (C1 or D1) in three animals and to all vibrissae in the fourth rat. The stimulation bristle was moved at three to four sweeps/sec from caudal to rostral. In the control groups, the stimulation apparatus was activated, but the bristle did not touch the animals.

At the end of the experiment, each rat was given a lethal dose of sodium pentobarbital (Nembutal, 100 mg/kg, i.v.). Vertical 26 gauge stainless steel oil-coated needles were inserted under stereotaxic guidance at sites 3.0 mm posterior to bregma and 3.0 mm to the left and right of the midline to make fiducial tracks for later coronal alignment. The brain was removed, and anteroposterior fiducial needle tracks were made in each hemisphere for registration of brain sections during subsequent imaging procedures. The brain was frozen in methyl butane at −35°C and cut on a cryostat at 30 μm into serial coronal sections throughout the striatum, from anteroposterior (AP) −2.0 to +2.0 mm relative to bregma (Paxinos and Watson, 1998). The sections were mounted on glass slides, and the slides were apposed to SB5 x-ray film and stored at −70°C in light-tight cassettes for 12–14 d. Films were developed with Ciné developer (White Mountain Imaging, Webster, NH). The sections were returned to −70°C and stored until [^{3}H]naloxone binding was performed.

[^{3}H]Naloxone ligand binding. [^{3}H]Naloxone binding was performed on sections previously processed for 2DG according to the procedure described by Moratalla et al. (1992). Briefly, the sections were allowed to come to room temperature and were then preincubated for 5 min at 4°C in 50 mM Tris-HCl buffer in 100 μM NaCl, which removed enough 2DG so that it was not detected by the film. They then were incubated for 60 min in 2.5 nM [^{3}H]naloxone (DuPont NEN). Controls for nonspecific binding were treated with a 1 μM solution of unlabeled naloxone hydrochloride (Sigma, St. Louis, MO). All slides were washed three times in 50 mM PBS, rinsed in distilled water, dried, and apposed to Hyperfilm-^{3}H (Amersham Biosciences, Arlington Heights, IL) for 5 weeks at room temperature before development with Ciné developer.

Image analysis of autoradiographic data. Reliable visualization and unbiased localization of peaks in 2DG autoradiograms representing increases in glucose utilization on the order of ≤20% required use of computer-assisted imaging techniques. To obtain an unbiased selection of peaks and an unbiased determination of their borders, we developed computer programs that automatically detected regions of peak metabolism as activity features in digitized 2DG images of the striatum (Fig. 1*A–A″,B–B″*). Other programs detected striosomes in the paired [^{3}H]naloxone images of the same sections (Fig. 1*C–C″*). The program for detection of 2DG peaks automated the thresholding method used in previous studies (Brown et al., 1996) to avoid the necessity for visual selection of "regions of interest" in 2DG images and provided a standardized method for assigning edges to the peaks.

Autoradiograms of coronal sections were digitized into 256 gray levels (0 = white, and 255 = black) with a Sony CCD camera and a Scion LG-3 frame grabber. The software was a Macintosh-based version of NIH Image written by Wayne Rasband at the National Institute of Mental Health (available from the Internet at http://rsb.info.nih.gov/nih-image). The two digitized images of each histologic section, one [^{3}H]naloxone and one 2DG, were registered in an image "stack" by means of a customized macro within NIH Image. Fiducial markers, salient features, and tissue artifacts were all used to align the autoradiographic images. The macro incorporated bilinear interpolation to rescale the [^{3}H]naloxone images to compensate for the shrinkage of the sections that occurred during tissue processing, relative to the 2DG labeling before the processing. The alignment procedure was repeated several times for each pair of images for each section. All measurements were performed bilaterally.

Algorithm for detection of local metabolic peaks. For detection of 2DG-labeled metabolic peaks, we used an algorithm designed to locate on a Cartesian grid the largest, most intensely labeled (darkest) peaks of radiolabeling in the striatum. In autoradiograms imaged at a resolution of 256 gray levels, the striatum contained ~50 gray levels that could be seen by eye to be heterogeneously distributed into light and dark patchy regions (Fig. 1*A,B*). This level of imaging is constrained by the resolution of the x-ray film, ~0.0025–0.01 mm^2 (50–100 linear μm; 2500–10,000 μm^2; Smith, 1983). The custom-written macro in NIH Image that we used for peak detection first applied a 7 × 7 Gaussian filter to smooth the deoxyglucose image and then selected the darkest striatal pixel as the starting point for autothresholding. A primary peak was then identified. Starting from the gray level of the darkest pixel, the left striatum was thresholded iteratively at successively lower gray levels until a peak was found that exceeded the preset minimum peak area (200 pixels = 0.116 mm^2, 0.340 linear mm, 115,600 μm^2), approximately the size of a circle with a diameter of 0.384 mm. This size criterion was reached by an initial analysis of >200 autoradiograms, which showed that this size minimum (well above the resolution of the film) avoided spurious small artifacts and resulted in separable activity peaks. The procedure followed is similar to a computer vision tool called scale-space primal sketch that has been used successfully in human metabolic mapping studies to localize functional activation (Lindeberg et al., 1999).

To define the limits of the detected primary peak, its final size was determined by its rate of growth during iterative thresholding. A sudden, rapid increase in the size of the feature during autothresholding indicated that the primary feature had merged with a smaller one. The strategy of restricting the primary metabolic peak to a feature size less than a maximum of 0.145 mm^2 that grows at a rate <0.029 mm^2 served to locate features with high-contrast edges. Features with low-contrast edges grow more quickly than do features with high-contrast edges when iterative thresholding at progressively lower values is applied. As a result, the high-contrast features can be selectively extracted by this step. We thus identified a primary peak in the striatal image as a cluster of pixels of limited size that had the darkest pixel and high contrast.

After a primary peak was identified, its threshold level was applied to the entire image, and the peak identification process was repeated. Between 1 and 20 secondary peaks were typically identified in the striatum of one hemisphere (Fig. 1*A″,B″*). They ranged in size from 0.0027 to 0.390 mm^2 with a mean of 0.053 mm^2. The original image was

then rotated 180° around its vertical axis, and the processing was repeated on the contralateral striatum.

Detection of [^{3}H]naloxone-positive striosomes. To locate the [^{3}H]naloxone-positive features in digitized autoradiograms, a second customized macro in NIH Image applied a 5 × 5 Gaussian filter to accentuate the contrast borders within the image and then smoothed the resulting image by application of a 5 × 5 mean filter. This image was then multiplied by the original image, and the result was scaled back to gray level values that range from 0 to 255. The program then found the high-contrast point in the gray level histogram of the image, where the histogram peak leveled off and included the darkest pixels. This gray level was used to detect striosomes, which were defined as features between 0.0058 and 5.81 mm^2 in the [^{3}H]naloxone autoradiogram (Fig. 1*C″*). The size criterion was determined by study of >200 autoradiograms and was easily validated by matching the size and shape of the clearly defined features in an image stack consisting of the original digitized [^{3}H]naloxone autoradiogram and the image that resulted from feature detection.

Combining 2DG and [^{3}H]naloxone features into a comparison image. After completion of feature extraction for the left and right striata for each section, the 2DG and [^{3}H]naloxone images were combined in a single comparison image to determine the extent to which the deoxyglucose and [^{3}H]naloxone features overlapped. A copy of the original digitized [^{3}H]naloxone image was taken as a template within which to place the 2DG and [^{3}H]naloxone features. The macro then used NIH Image utilities to calculate the feature areas of each type and the percentage of the total [^{3}H]naloxone feature pixels that overlapped the 2DG features. It also assigned colors to these values via a color lookup table, which helped in viewing the features and regions of overlap. The centroid position (*x* and *y* coordinates) and area (square millimeters) of each 2DG peak, each striosome, and each region of overlap were measured in the dorsal half of the striatum in comparison images throughout the striatum using the NIH Image macro. Positions were calculated in millimeters relative to lines marking the midline and the dorsal edge of the striatum. Once the peaks and striosomes in the dorsal striatum had been selected, their areas were measured separately, as well as their percent overlap. Percent overlap of the total 2DG peak area with striosomes was calculated separately from percent overlap between the 2DG peaks and total striosome area. In addition to defining overlaps of 2DG peaks and striosomes in this manner, we also systematically increased the sizes of the 2DG peaks to the point at which striosomes were included.

Statistics. The centroids of all peaks were plotted on atlas diagrams of sections in horizontal, coronal, and sagittal planes (Paxinos and Watson, 1998). Large differences were noted by visual inspection. To compare metabolic peak location results statistically, we used a mixed models repeated measures analysis of covariance on the *x* and *y* variables (MANCOVA; criterion $p < 0.05$) followed by *t* tests to compare individual groups of animals (SAS software, version 6.12, spatial statistics, mixed model; SAS Institute, Inc., Cary, NC). The *t* tests reported were all planned comparisons. AP levels (the *z* variable) were divided into six ranges relative to bregma, in 300, 400, 500, and 600 μm blocks: AP −2.0 to −1.5, −1.5 to −1.0, −1.0 to −0.3, −0.3 to +0.1, +0.1 to + 0.4, and +0.4 to +1.0 mm. These ranges span known corticostriatal projection patterns from SI cortex in the rat (Brown et al., 1998; Alloway et al., 1999).

Immunohistochemistry for anterograde tracer studies and deoxyglucose autoradiography. In four additional rats, biotinylated dextran amine (BDA) was injected into electrophysiologically identified sites in SI cortex (Brown et al., 1998; $n = 3$, HL; $n = 1$, FL), and a 2DG experiment was performed 2 weeks after the injections. A 2 week delay was necessary to allow cortical metabolism to return to normal after the surgery. At the end of the 45 min experimental DG period, the rats were perfused with 0.9% saline and 10% neutral buffered formalin, and fiducial markers made of stainless steel tubing were placed anteroposteriorly in the brains. Cryostat sections were cut at 30 μm, and sections were alternately mounted on slides or placed in individual wells containing PBS. The sections on slides were apposed to film for autoradiography, and the sections in PBS were processed for BDA immunohistochemistry (Bevan et al., 1997). The BDA sections were floated onto slides, and both the DG autoradiograms and matching BDA-stained sections were digitized. Metabolic peaks were detected and outlined onto the two sets of images, and they were aligned by means of the fiducial markers and the external capsule. The images showed that these procedures resulted in local diffusion of label so that individual axons were not visible. However, projection fields were readily identifiable.

RESULTS

Rats in the free-movement groups sat quietly in the observation chamber, only occasionally grooming or otherwise moving ("quiet group"), or, for the rats in cages, ate chocolate more than half of the time or otherwise rested or groomed ("active group"). Striatal glucose utilization in the striatum of these rats included regions of relatively lower and higher glucose utilization rates compared with the average rate of the entire striatal region sampled, as described previously (Brown, 1992; Brown and Sharp, 1995; Brown et al., 1996). The metabolic peaks (115 ± 10 compared with 91 ± 9 $\mu mol \cdot 100\ gm^{-1} \cdot min^{-1}$ for the average) were readily identified by the algorithm (Fig. 1*A″*) and appeared throughout the striatum. In the quiet group there was a 300- to 500-μm-wide lateral zone with fewer peaks than found in the same location in rats that moved about and ate (Fig. 2*A,B*). In the group of lightly restrained rats, metabolic peaks were also widely distributed, but the conditions of restraint affected the distributions, especially laterally (Fig. 2*C,E,G*). Peak locations in the restrained HL, FL, and VIB control groups were different from each other ($p < 0.01$–0.05, depending on the AP level, MANCOVA and *t* tests).

Metabolic activity in the striatum of rats given tactile stimulation was heterogeneous as in the controls (Fig. 1*B*), but the highest metabolic peaks in these animals clearly occurred in the far lateral part of the striatum, corresponding to the sensorimotor sector (Fig. 2*D,F,H*; Brown, 1992). Mean ± SEM glucose utilization of the peaks was 105 ± 9 $\mu mol \cdot 100\ gm^{-1} \cdot min^{-1}$ compared with the average of 96 ± 8.

The peak distributions in the striatum in all of the stimulation groups were statistically different from those in their respective restraint controls from AP −1.0 to +1.0 mm ($p < 0.05$ for VIB vs VIB control; $p < 0.005$ for HL vs HL control and FL vs FL control; MANCOVA and *t* tests). Compared with the distributions in the quiet free-movement rats, the patterns in the VIB group were different at AP −1.5 to −1.0 and −0.3 to +1.0 ($p < 0.05$), and the distributions in the HL and FL stimulation groups were different at most AP levels from −1.0 to +1.0. Thus, differences related to the applied somatosensory stimulation occurred over a 2.5 mm range but not at all levels within that range for each group.

Comparison of striatal metabolic activity distributions and the distribution of striosomes

The results of the compartmental analysis were clear-cut: there was minimal overlap of the peaks of metabolic activity with striosomes in any of the rats, whether they had been free-moving, lightly restrained, or stimulated under light restraint (Fig. 3). In 30% of the sections analyzed, there was no overlap whatsoever. The mean percentages of the total striosomal area coincident with DG peaks per section were 3.4 ± 0.2% (left) and 3.5 ± 0.2% (right) for the free-movement rats and were 3.5 ± 0.2% (left) and 3.4 ± 0.2% (right) for the restraint controls. For stimulated animals, the overlap was nearly identical: 3.0 ± 0.2% (left), ipsilateral to the side of stimulation, and 2.9 ± 0.2% (right), contralateral to the side of stimulation. The mean percentages of the total DG peak area containing striosomes were 6.7 ± 0.4% (left) and 6.8 ± 0.5% (right) for the free-moving rats, 6.4 ± 0.4% (left) and 5.2 ± 0.5% (right) for the lightly restrained rats, and 6.3 ± 0.3% (left) and 6.3 ± 0.3% (right) for stimulated animals. There were no differences in striosome peak overlap among the stimulated groups.

Nearly all overlap that did occur between peak metabolic

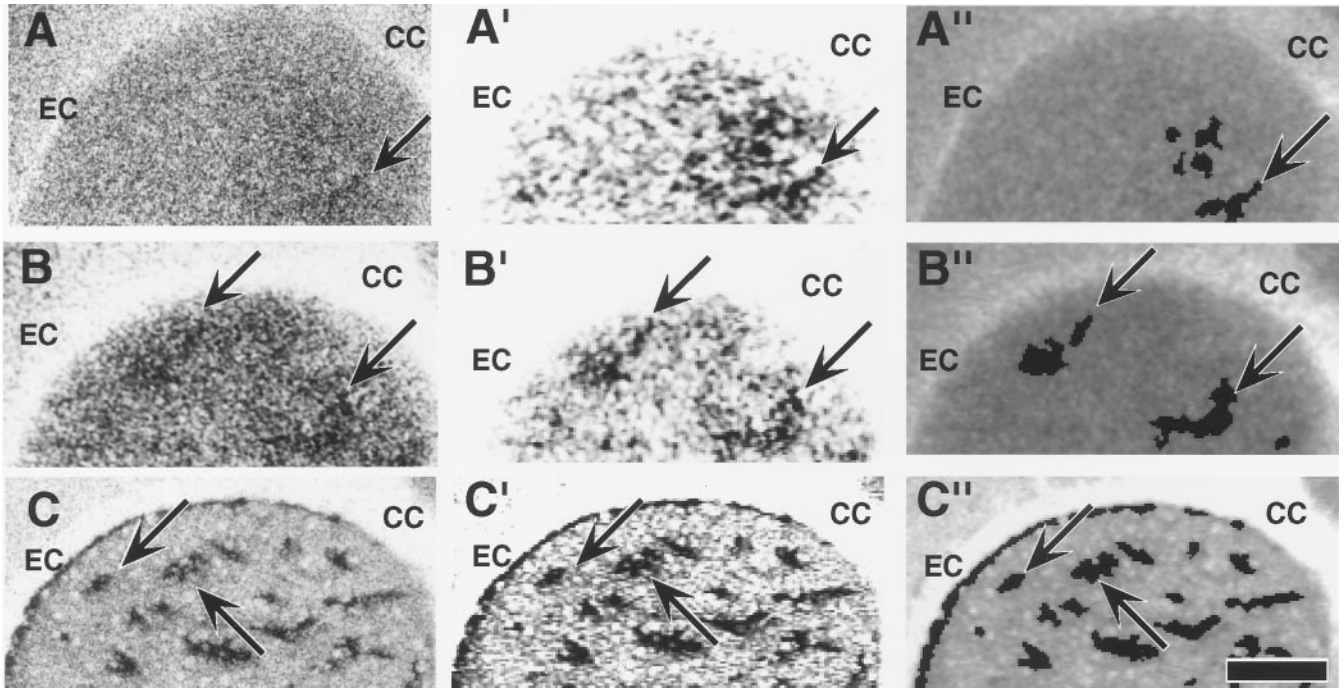

Figure 1. Computer-based detection of peak glucose utilization rate and striosomes in [^{14}C]DG and [^{3}H]DG autoradiograms of the striatum. *A*, [^{14}C]2DG autoradiogram of transverse sections through the left striatum of an unstimulated, lightly restrained control rat. The *arrow* indicates a medial region of relatively high activity. *B*, Autoradiogram at a similar level from a rat that received tactile stimulation of the hindlimb. *Arrows* indicate medial (*right*) and lateral (*left*) regions of highest metabolic activity estimated by visual inspection. Note that metabolism is heterogeneous in the control as well as the stimulated animal; the effect of stimulation is determined by the location of the peaks that are unique to the stimulated group, in this case the lateral striatum. *C*, [^{3}H]Naloxone autoradiogram of the same section illustrated in *B* after washout of the ^{14}C that had been in the tissue, which permitted detection of the [^{3}H]naloxone binding. *Arrows* indicate two of the μ-opioid receptor-rich striosomes. *A′–C′*, Digitized and enhanced images of sections shown in *A–C*. Standard image processing (equalization) shows the darkest regions in the autoradiograms (*arrows*) as peaks (*A′, B′*) or striosomes (*C′*). *A″–C″*, A computerized algorithm detected metabolic peaks (*A″, B″*) and striosomes (*C″*), shown as *black* features on images of the brain sections. Note that although the original ^{14}C-labeled autoradiograms have no sharp feature edges, the algorithm located the largest, darkest, clearly separable features. The *top left arrow* in *B″* indicates a metabolic peak in the lateral striatum that was absent in the control shown in *A″*. This peak location, found reliably in all stimulated animals, corresponded to a hindlimb sensorimotor cortex input zone. *CC*, Corpus callosum; *EC*, external capsule. Scale bar, 500 μm.

activity and striosomes was at the edges of the striosomes or at out-jutting parts of the striosomes or involved very small striosomal features (Figs. 3*C–F*, 4*A*). We estimate that the overlap was no more than 1–20 μm. Of all the DG peaks measured in the free-moving, restrained, and stimulated animals, 40% overlapped a striosome in this minimal manner. This overlap could have resulted from errors intrinsic to our overlay method, which included correction for shrinkage and relied on fiducial points that were not immediately adjacent to the features compared. There were rare instances of complete overlap (3 of 2603 overlap instances measured) fitting the size and shape of striosomes exactly, which indicated that the method we used could detect peak activity in striosomes were it present. These instances were not associated with any behavioral group.

As a check on our single-section comparison method, we chose from a HL stimulation case a single metabolic peak in the DG image that lay next to a striosome and aligned it with the corresponding peaks in nine consecutive serial sections (Fig. 3*G,H*). The small amount of overlap of the metabolic peak with the striosome noted in the original section did not expand to overlap the striosome significantly, and the overlap sites did not form larger areas than those seen in single sections did.

We performed a detailed analysis to determine how critical the border assignments for the metabolic peaks were to the results (Fig. 4). We systematically increased the image area of the metabolic peaks in individual sections in two to four animals from each treatment group. We reasoned that if the observed overlap were a random process, then it would follow a linear function ($y = x$). When peak image sizes were increased by progressively lowering the threshold for peak gray levels across the entire range for detection of metabolic activity, the overlap of metabolic peaks and striosomes did not increase beyond 10% until the detection threshold was set below a gray level that could distinguish individual peaks (Fig. 4*A*). Accordingly, plotting overlap as a function of percentage detected was not linear until the background was detected (Fig. 4*B*). In contrast, when we generated sets of randomly distributed peak images for individual brain sections (Fig. 4*C*) and randomly distributed 100 sets of the peaks on a template of the striosomes for that section, overlap with striosomes was substantial (Fig. 4*D*) and significantly greater for the randomly distributed sets than for the actual peaks detected ($p < 0.00007$).

Comparison of metabolic activity distributions and matrisomes

We analyzed SI inputs labeled by BDA injections placed at electrophysiologically identified sites in SI cortex representing the hindlimb ($n = 3$) and forelimb ($n = 1$) in relation to metabolic peaks labeled by somatotopically matched HL and FL stimulation at the periphery performed in the same animals.

The direct matrisome–metabolic peak comparisons (Fig. 5) demonstrated predominant overlap of the cortical input zones

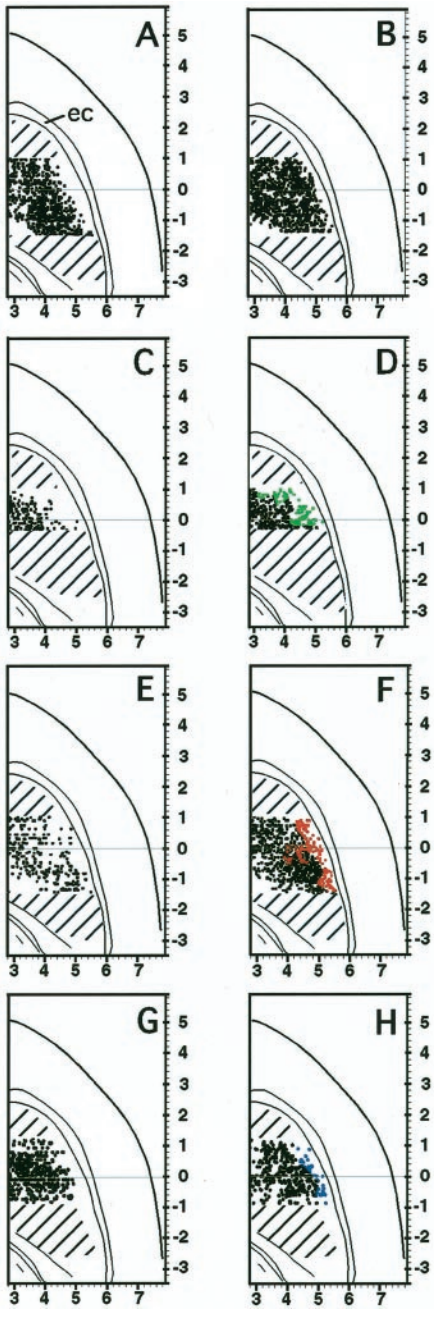

Figure 2. Distribution of metabolic peaks in the striatum in the quiet and free-movement groups and in the restrained control and stimulation groups. Centroids of peaks are shown as *dots*. The drawings illustrate the 2.5 mm anteroposterior range in which the peak distribution (*dots* drawn on *horizontal sections*) in the comparison groups were statistically different. The far lateral striatum was especially activated by movement and somatosensory stimulation. *Color dots* indicate the area of lateral peaks not present in restraint controls. *A*, Quiet group. *B*, Active group. Peaks appear farther laterally in the striatum in the active than in the quiet animals. The same was true for stimulated versus restraint controls for HL stimulation (*C*, restraint control; *D*, stimulated), VIB (*E*, restraint control; *F*, stimulated), and FL (*G*, restraint control; *H*, stimulated) stimulation groups. *ec*, External capsule. The template for the *horizontal sections* is modified from Paxinos and Watson (1998) at interaural 5.26 mm. Scales are in millimeters.

and the peak zones of metabolic activity. The BDA labeling in sections processed for 2DG showed diffusion of a reaction product so that our estimates of overlap did not have single-fiber resolution. Even so, there was striking consistency in overlap of the metabolic peaks and BDA-labeled cortical inputs. Figure 5 illustrates this pattern in a HL case. The largest metabolic peak almost exactly matched the BDA labeling in size, shape, and location. Altogether, in the three HL rats and one FL rat, there was direct overlap of the metabolic peaks and lateral striatal projection fields in 60–80% of the sections collected from AP −1.0 to AP +1.7 mm. In contrast, in the medial striatum, to which SI cortex projects minimally, there was no overlap in one HL rat and the FL rat and one small peak overlapping a BDA-labeled zone in the other HL rats.

DISCUSSION

Our findings demonstrate that the highest metabolic activity in the striatum occurs in the matrix compartment rather than in striosomes in awake behaving animals under a range of behavioral conditions, including voluntary movement, light restraint, and focal stimulation of different parts of the body surface. Like other imaging techniques depending on metabolic activity or blood flow (Hevner et al., 1995; Disbrow et al., 2000; Gsell et al., 2000; Nakao et al., 2001), the 2DG method is an indirect measure of neural activity and is not sensitive to phasic activity states. Nevertheless, in a variety of other experimental conditions, it has been closely correlated with neuronal activity, especially at axon terminals (Hubel et al., 1978; Mata et al., 1980; Yarowski et al., 1983; Ackermann et al., 1984). Our finding that activity predominates in the matrix throughout the striatum during resting and neutral behavioral states suggest that the neurochemically distinguished striosome and matrix compartments of the striatum represent not only anatomically distinct subdivisions of the striatum but also subdivisions that can have differential rather than coordinate activity during natural behaviors. Specifying the nature of the behavioral states that coordinately or independently activate these striatal compartments could have major implications for understanding the normal functions of the basal ganglia and their dysfunction in extrapyramidal disorders.

Metabolic activity in the matrix predominates during voluntary movement and quiet restraint

A striking finding in our study is that even in rats free to move about, groom, or eat, peak metabolic activity occurred preferentially in the matrix compartment and not in striosomes. This result held for the entire striatum, suggesting that under relatively natural conditions of free movement or rest, the dominant activity of axon terminals in the striatum is in the matrix compartment.

It is unlikely that the matrix predominance of peak metabolic activity resulted from a failure of the technique to detect large overlaps between metabolic peaks and striosomes, because there were very rare instances of extensive overlap detected and numerous instances of overlap of a few micrometers at striosomal borders, nor could the low level of activity in striosomes simply have reflected a failure of our technique to measure peaks as small as striosomes, because the areas of the metabolic peaks and striosomes were very similar, and both had irregular edges within the detection threshold. The possibility remains that activity was elicited in striosomes but at levels below our background values or in phasic episodes too brief to be detected.

Interestingly, we did find very slight overlaps between the edges of metabolic peaks and the edges of striosomes. We were unable

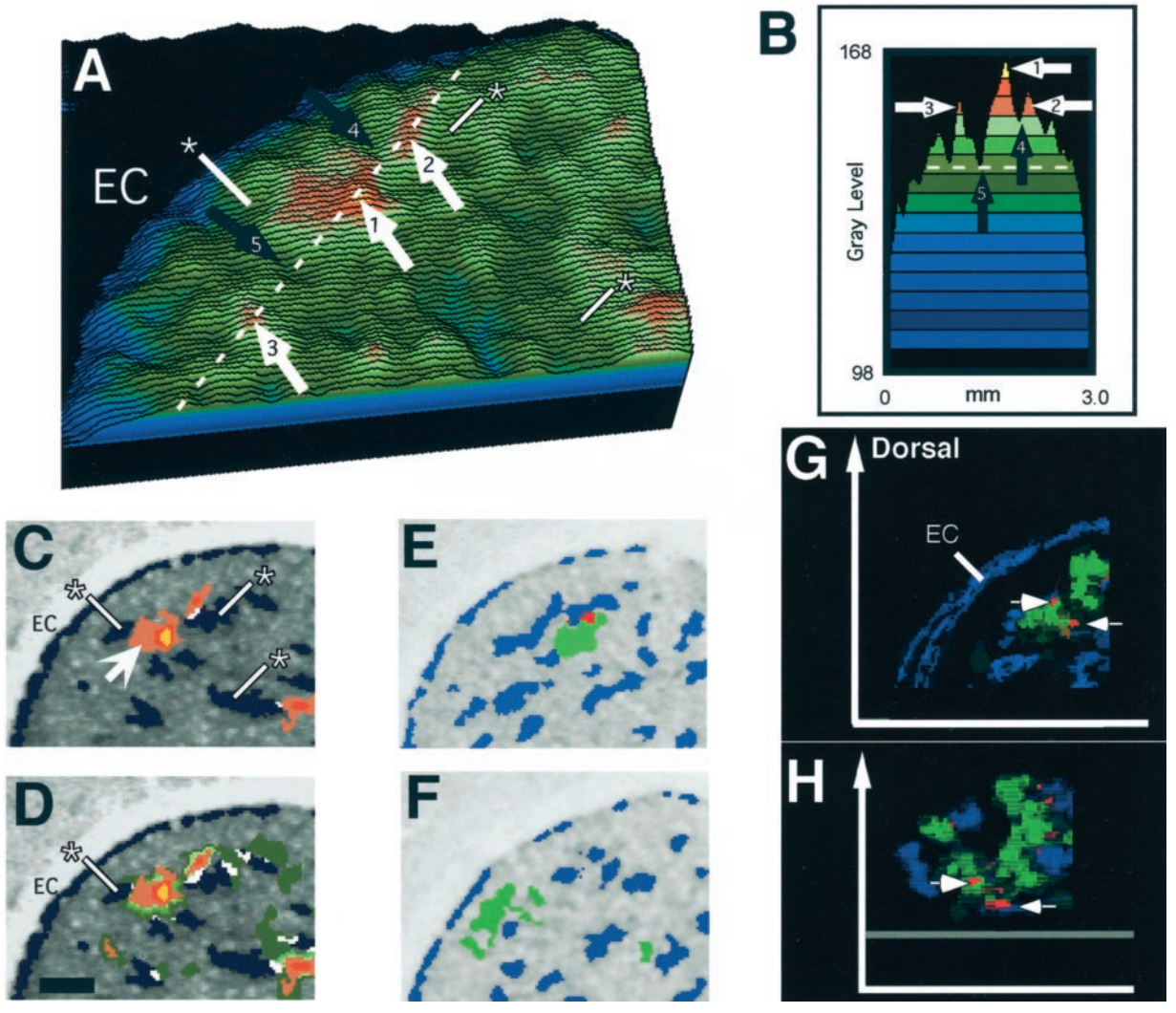

Figure 3. Metabolic peaks in the striatum of stimulated and free-movement animals overlap minimally with striosomes. *A*, Surface plot of the dorsolateral striatum in a HL-stimulated animal (shown in Fig. 1*B*), color-coded to illustrate the peaks and valleys formed by the high and low gray levels that represent glucose utilization rates. The gray level of the *yellow–brown peak* (*white arrow 1*) is 20% higher than the gray level of the baseline measured at *black arrow 5*, which is the mean gray level measured for the entire striatum. The *white dotted line* indicates the level of the cross-section shown in *B*. The *white arrows* indicate the peaks, and the *black arrows* indicate the valleys that correspond to those shown in *B*. *B*, Profile of gray levels plotted along the *white dotted line* in *A*. Each *color* represents four gray levels. The program used for peak detection first detects the darkest pixels (*yellow*) and then progressively lowers the threshold to include the gray levels shown in the *browns* and *greens*. In this example, when the gray levels in the *light green* range are detected, the two largest peaks merge across the valley indicated by *black arrow 4*. The program then chooses the level of detection that does not merge the two peaks. *C*, Image of the metabolic peaks detected in *A* overlaid on the autoradiogram with labeled striosomes. The program detected two peaks in the dorsolateral striatum (*arrow*), color-coded according to the plot profile and surface plots in *A* and *B*. The region of highest metabolism is shown in *yellow*. *Asterisks* show examples of striosomes (*blue*; compare locations in *A* and *C*). *D*, Same image as in *C*, except that the detection level was set to include gray levels well below those illustrated in *C*. Accordingly, the program detected larger peaks than those shown in *C*, which allowed the peaks to merge but still produced very little overlap (*white*) with striosomes. *E, F*, Two examples of minimal or no overlap in the free-movement group. Metabolic peaks (*green*) avoid striosomes (*blue*) or show overlap (*red*). *G*, Three-dimensional rendering of 10 serial sections (30 μm each; 300 μm total) in the anterior striatum illustrating two stimulus-specific metabolic peaks (*green*) and striosomes (*blue*). Regions of overlap are shown in *red*. *H*, Same 10-section reconstruction rotated forward 75° around the *x*-axis to illustrate the view from the dorsal surface of the striatum. The *arrows* indicate the same small regions of overlap shown in *G* and *H*. Reconstructions and three-dimensional renderings were made using VoxBlast software (Vaytek Inc., Fairfield, IA). *EC*, External capsule. Scale bar, 500 μm.

to determine whether this slight overlapping indicated true peristriosomal activation or errors of alignment, but rims around striosomes have been noted repeatedly in anatomical studies (Graybiel and Ragsdale, 1978; Faull et al., 1989; Graybiel, 1996; Jakab et al., 1996; Waldvogel et al., 1999). These boundary zones could be functionally important regions for striatal processing involved in learning and transforming neutral inputs related to motivationally important signals (Aosaki et al., 1995).

The strong metabolic activity in the matrix that occurred during free movement, quiet rest, and quiet restraint could reflect the broad array of cortical and thalamic inputs that reach the matrix compartment. The matrix receives most corticostriatal inputs from sensory cortices, from motor and premotor areas, and from the association cortex and also much of the large thalamic input to the striatum (Donoghue and Herkenham, 1986; Malach and Graybiel, 1986; Flaherty and Graybiel, 1991; Ragsdale and Graybiel, 1991; Kincaid and Wilson, 1996; Brown et al., 1998). As the free-movement rats moved about, rested, or engaged in grooming

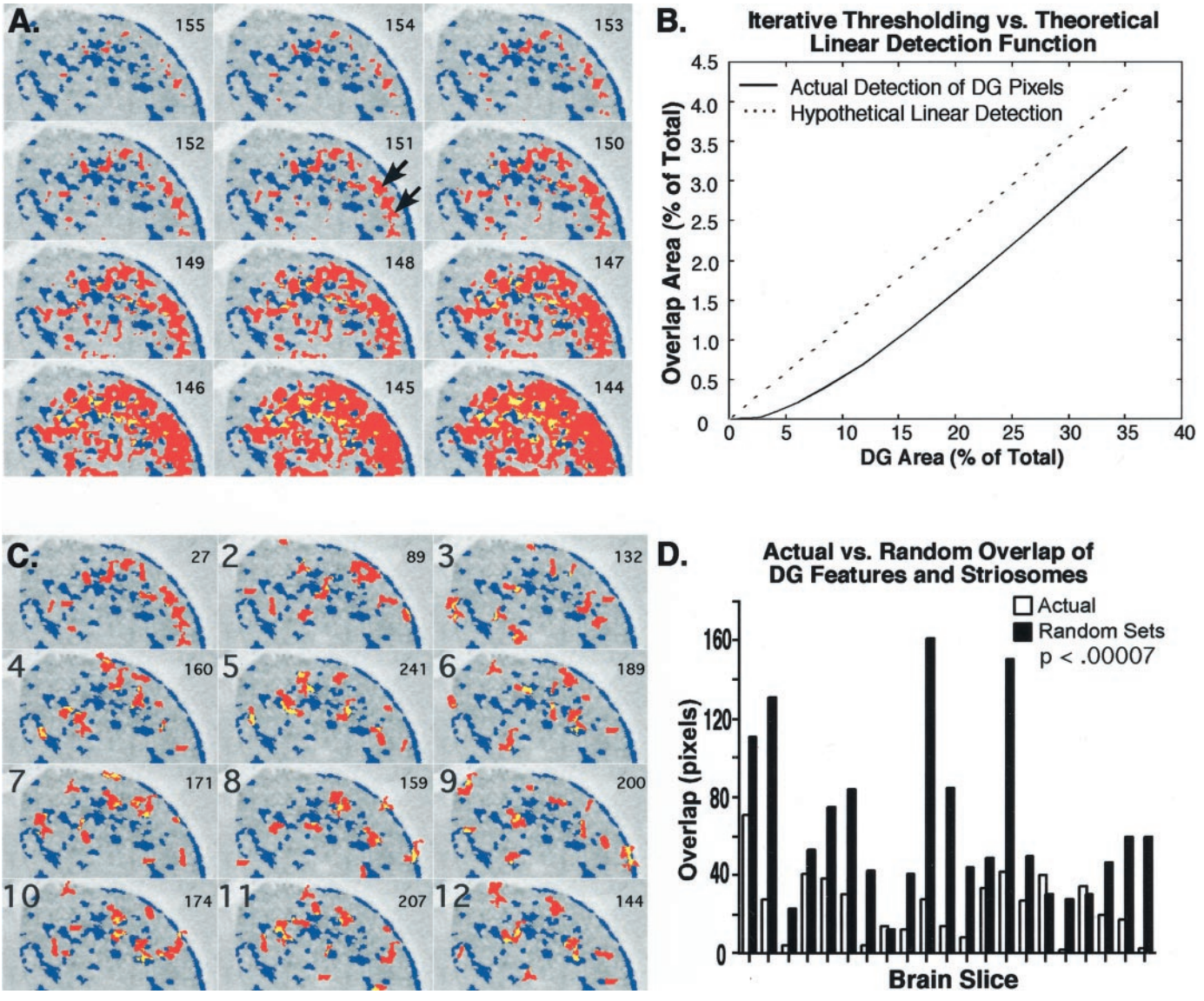

Figure 4. Restriction of metabolic peaks to the striatal matrix after tactile stimulation. *A*, *Panels 155–144* (*numbers* at *top right*) show digitized images of the right striatum from a single section from an FL stimulation case, subjected to iterative thresholding from gray level 155 to gray level 144. Even when metabolic peak detection was increased to include most of the dorsolateral striatum, the progressively lower rates of glucose utilization included still lay within the matrix. The DG peaks (*red*) were superimposed on a template of striosomes (*blue*) detected in the same transverse section by [^{3}H]naloxone binding. Overlap is shown in *yellow*. The *arrows* in *panel 151* indicate the peaks associated with FL stimulation according to comparisons with controls. The gray level in *panel 151* was chosen by the algorithm for measurement of peak feature size. *B*, Plot of the overlap of DG peaks with [^{3}H]naloxone-positive striosomes (*solid line*) and a hypothetical linear function for overlap (*dotted line*). The actual overlap is nonlinear at <8% DG detection (A, *panels 155–149*). *C*, *Panels 2–12* show 11 artificial, randomly distributed sets of DG features superimposed on the same template as in *A*. The *first panel* illustrates the actual data. The number of pixels in which DG peaks (*red*) and striosomes (*blue*) overlap is shown in the *top right*. The area of overlap in the *first panel* with actual data (27 pixels) is less than in any of the randomly distributed sets (89–241 pixels; each pixel = 24 μm). *D*, Comparison of the overlap of striosomes with peaks detected in actual cases (*white bars*) and with artificial, randomly distributed peaks (*black bars*). The 21 pairs of *bars* are data derived from transverse sections through the striatum in 11 rats. For each section, overlap with [^{3}H]naloxone-positive striosomes was measured for 100 sets of actual peaks and for these peaks given randomly generated locations. *Bars* represent median overlap; overlap of the randomly distributed features was significantly greater (64.3 vs 23.7 pixels; $p < 0.0007$).

or feeding behaviors, these inputs appeared to have predominated. In the one electrophysiological study differentiating neuronal activity in striosomes and matrix during open-field behavior, the neurons activated were also found in the matrix (Trytek et al., 1996). A large part of the striatal neuropil is made up of the processes of intrinsic neurons, so that the strong metabolic activity in the matrix could also reflect such local circuit function (Kawaguchi et al., 1995). Our results suggest that the activity of such intrinsic circuitry also did not blur or abolish the matrix predominance of functional metabolic activity.

The near absence of peak metabolic activity in striosomes in this study suggests that strong or sustained striosomal activation or both may require special behavioral circumstances. Unlike the matrix, striosomes receive strong cortical inputs preferentially from posterior orbital and anterior cingulate and caudal prefrontal cortical areas, regions that have been associated with limbic and evaluative circuits of the forebrain (Donoghue and Herkenham, 1986; Ragsdale and Graybiel, 1990; Eblen and Graybiel, 1995; Ferry et al., 2000). Indirect evidence has implicated striosomes in motivation-based processing and the development of

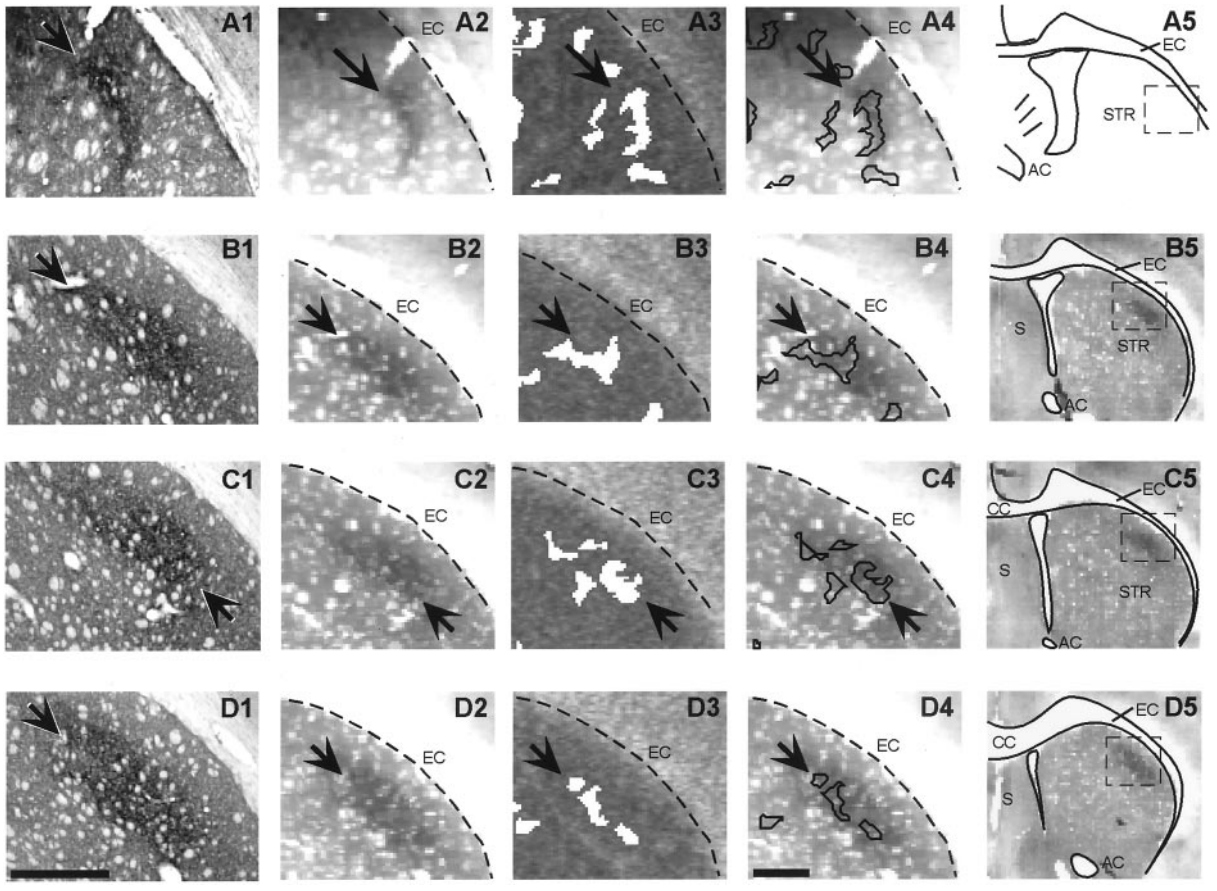

Figure 5. Anatomically identified matrisomes and neural activity coincide over a wide anteroposterior extent of the sensorimotor striatum. Corticostriatal inputs from the hindlimb region of cortex were labeled with BDA (*A1–D1*), and 2DG maps of the striatum were made after HL stimulation. *Row A* and *rows B–D* are from two different rats. Each *row* shows a different anteroposterior level, ranging from −0.8 to +1.0 mm relative to bregma. BDA-labeled terminal arborization fields are indicated by *arrows*. *A2–D2*, Digitized versions of the BDA-stained sections at a size and resolution comparable with those of the adjacent section 2DG autoradiograms. *A3–D3*, Metabolic peaks (*white*) detected in adjacent section 2DG autoradiograms after tactile stimulation of the contralateral hindlimb. *A4–D4*, Outlines of the metabolic peaks in *A3–D3* overlaid on images of the BDA-stained sections, showing good correspondence between the anatomic HL projection field and the largest HL metabolic peaks. *A5*, The *dashed rectangle* indicates the region shown in the preceding panels. *B5–D5*, Low-power views of sections shown in B1-D1. *AC*, Anterior commissure; *CC*, corpus callosum; *EC*, external capsule; *S*, septum; *STR*, striatum. Scale bars, 500 μm.

behavioral focus (Aosaki et al., 1995; Houk et al., 1995; White and Hiroi, 1998; Graybiel et al., 2000). For example, striosomes have been identified as sites that sustain intracranial self-stimulation (White and Hiroi, 1998). In studies with early gene markers of activity, striosome-predominant activation has been found under conditions in which repetitive movements are induced by intense stimulation of dopamine receptors with agonist drugs (Canales and Graybiel, 2000) and, in experimental parkinsonism, when dyskinesias are induced by agonist treatments (Cenci et al., 1999; Saka et al., 1999). Activation of the striosomal compartment might have been weak in the animals studied here, because they were neither trained to engage in motivation-based or reward-seeking behaviors nor engaged in forced, repetitive, or stereotyped behaviors. In the free-movement groups, animals rested, briefly groomed or explored, or ate chocolate, and the restrained animals rested quietly without exhibiting agitation, whether receiving tactile stimulation or not.

Tactile stimulation elicits peak metabolic activity in matrisomes in the sensorimotor striatum

Within the matrix compartment, corticostriatal inputs from SI cortex terminate predominantly in patchy zones called matrisomes. Our findings provide the first evidence that these anatomically identified input matrisomes can be specifically and selectively activated by natural sensory stimulation. There was predominant overlap of metabolic peaks and BDA fibers labeled from small injection sites made in somatotopically corresponding SI sites and some near-total matches of the two labels, despite the technical problem of local diffusion of the BDA introduced by the conjoint 2DG processing. The overlap was well within the limits observed in previous experiments in which electrical stimulation of the somatosensory or motor cortex has been shown to activate local clusters of striatal neurons (Liles and Updyke, 1985; Parthasarathy and Graybiel, 1997).

It was not obvious that this predominant alignment of peaks and SI input patches would occur, given that the 2DG peaks likely reflect the activity of inhibitory as well as excitatory terminals and thus could have represented the local inhibitory network of the striatum (Kawaguchi et al., 1995; Koos and Tepper, 1999) as well as the stimulated afferents themselves. Our results suggest that whatever anatomical cross-connections do exist locally do not blur matrisome-predominant patterns of peak functional activity excited by stimulation at the periphery, nor, apparently, do the

diffuse systems of corticostriatal projections identified in several studies (Malach and Graybiel, 1986; Cowan and Wilson, 1994; Kincaid and Wilson, 1996; Wright et al., 1999). Other behavioral conditions might evoke other patterns of activity, but these results strongly support the hypothesis that matrisomes represent a functional substructure in the matrix compartment and suggest that the striatum uses modular processing of ongoing somatosensory inputs in the waking state.

Behavior-dependent activation of striatal compartments

The striatum is the main input station of the basal ganglia. How the striatum responds in behavioral situations is, therefore, likely to be a crucial determinant of how the basal ganglia process information to affect motor and cognitive functions. Our results suggest that the balance of synaptic activity between striosome and matrix compartments favors the matrix in neutral behavioral states, including free movement and quiet rest and during passive restraint either alone or with focal tactile stimulation. The matrix compartment gives rise to the direct and indirect output pathways of the basal ganglia, which operate to control basal ganglia outflow to the neocortex and brainstem. For the motor system, these pathways have been shown to constitute an opponent mechanism to engage in selecting and releasing movements (Mink, 1996). These patterns likely have comparable opponent functions in modulating cognitive activity (Swerdlow and Koob, 1987; Graybiel, 1997; Bejjani et al., 1999). Thus, under many conditions, the matrix–direct–indirect pathway system may dominate striatal activity. Striosomes, in contrast, have the special property of projecting to the region of the dopamine-containing substantia nigra pars compacta (Gerfen, 1985; Jiménez-Castellanos and Graybiel, 1989). They thus may be active in the modulation of dopamine-containing inputs to the basal ganglia, including the modulation of the reward-based signals that are thought to be carried by these dopaminergic fibers (Schultz and Romo, 1988). This property suggests that they may be part of an architecture contributing to learning and memory functions of the basal ganglia (Graybiel and Kimura, 1995; Houk et al., 1995; Brown et al., 1999). Our findings do not address the issue of learning-based activity in the striatum but do strongly suggest that striosomes and matrix have distinct patterns of activation in the course of normal voluntary behavior.

REFERENCES

Ackermann RF, Finch DM, Babb TL, Engel Jr J (1984) Increased glucose metabolism during long-duration recurrent inhibition of hippocampal pyramidal cells. J Neurosci 4:251–264.

Alexander GE, Crutcher MD (1990) Functional architecture of basal ganglia circuits: neural substrates of parallel processing. Trends Neurosci 13:266–272.

Alloway KD, Crist J, Mutic JJ, Roy SA (1999) Corticostriatal projections from rat barrel cortex have an anisotropic organization that correlates with vibrissal whisking behavior. J Neurosci 19:10908–10922.

Aosaki T, Kimura M, Graybiel AM (1995) Temporal and spatial characteristics of tonically active neurons of the primate's striatum. J Neurophysiol 73:1234–1252.

Bejjani B, Damier P, Arnulf I, Thivard L, Bonnet A, Dormont D, Cornu P, Pidoux B, Samson Y, Agid Y (1999) Transient acute depression induced by high-frequency deep-brain stimulation. N Engl J Med 340:1476–1480.

Bevan MD, Clark NP, Bollam JP (1997) Synaptic integration of functionally diverse pallidal information in the entopeduncular nucleus and subthalamic nucleus in the rat. J Neurosci 17:308–324.

Brown J, Bullock D, Grossberg S (1999) How the basal ganglia use parallel excitatory and inhibitory learning pathways to selectively respond to unexpected rewarding cues. J Neurosci 19:10502–10511.

Brown LL (1992) Somatotopic organization in rat striatum: evidence for a combinatorial map. Proc Natl Acad Sci USA 89:7403–7407.

Brown LL, Sharp FR (1995) Metabolic mapping of rat striatum: somatotopic organization of sensorimotor activity. Brain Res 686:207–222.

Brown LL, Hand PJ, Divac I (1996) Representation of a single vibrissa in the rat neostriatum: peaks of energy metabolism reveal a distributed functional module. Neuroscience 75:717–728.

Brown LL, Smith DM, Goldbloom LM (1998) Organizing principles of cortical integration in the rat neostriatum: corticostriate map of the body surface is an ordered lattice of curved laminae and radial points. J Comp Neurol 392:468–488.

Canales JJ, Graybiel AM (2000) A measure of striatal function predicts motor stereotypy. Nat Neurosci 3:377–383.

Carelli RM, West MO (1991) Representation of the body by single neurons in the dorsolateral striatum of the awake, unrestrained rat. J Comp Neurol 309:231–249.

Cenci M, Tranberg A, Andersson M, Hilbertson A (1999) Changes in the regional and compartmental distribution of FosB- and JunB-like immunoreactivity induced in the dopamine-denervated rat striatum by acute or chronic L-dopa treatment. Neuroscience 94:515–527.

Cowan RL, Wilson CJ (1994) Spontaneous firing patterns and axonal projections of single corticostriatal neurons in the rat medial agranular cortex. J Neurophysiol 71:17–32.

Crane AM, Porrino LJ (1989) Adaptation of the quantitative 2-[^{14}C]deoxyglucose method for use in freely moving rats. Brain Res 499:87–92.

Crutcher MD, DeLong MR (1984) Single cell studies of the primate putamen. I. Functional organization. Exp Brain Res 53:233–243.

Disbrow EA, Slutsky DA, Roberts TPL, Krubitzer LA (2000) Functional MRI at 1.5 tesla: a comparison of the blood oxygenation level-dependent signal and electrophysiology. Proc Natl Acad Sci USA 97:9718–9723.

Donoghue JP, Herkenham M (1986) Neostriatal projections from individual cortical fields conform to histochemically distinct striatal compartments in the rat. Brain Res 365:397–403.

Durham D, Woolsey TA (1977) Barrels and columnar cortical organization: evidence from 2-deoxyglucose (2-DG) experiments. Brain Res 137:168–174.

Eblen F, Graybiel AM (1995) Highly restricted origin of prefrontal cortical inputs to striosomes in the macaque monkey. J Neurosci 15:5999–6013.

Faull RLM, Dragunow M, Villiger JW (1989) The distribution of neurotensin receptors and acetylcholinesterase in the human caudate nucleus: evidence for the existence of a third neurochemical compartment. Brain Res 488:381–386.

Ferry A, Ongur D, An X, Price J (2000) Prefrontal cortical projections to the striatum in macaque monkeys: evidence for an organization related to prefrontal networks. J Comp Neurol 3:447–470.

Flaherty AW, Graybiel AM (1991) Corticostriatal transformations in the primate somatosensory system. Projections from physiologically mapped body-part representations. J Neurophysiol 66:1249–1263.

Flaherty AW, Graybiel AM (1994) Input-output organization of the sensorimotor striatum in the squirrel monkey. J Neurosci 14:599–610.

Friedman HR, Goldman-Rakic PS (1994) Coactivation of prefrontal cortex and inferior parietal cortex in working memory tasks revealed by 2DG functional mapping in the rhesus monkey. J Neurosci 14:2775–2788.

Gerfen CR (1985) The neostriatal mosaic. I. Compartmental organization of projections from the striatum to the substantia nigra in the rat. J Comp Neurol 236:454–476.

Gerfen CR (1989) The neostriatal mosaic: striatal patch-matrix organization is related to cortical lamination. Science 246:385–388.

Gerfen CR (1992) The neostriatal mosaic: multiple levels of compartmental organization. Trends Neurosci 15:133–139.

Giménez-Amaya J-M, Graybiel AM (1991) Modular organization of projection neurons in the matrix compartment of the primate striatum. J Neurosci 11:779–791.

Graybiel A, Canales J, Capper-Loup C (2000) Levodopa-induced dyskinesias and dopamine-dependent stereotypes: a new hypothesis. Trends Neurosci 23:S71–S77.

Graybiel AM (1990) Neurotransmitters and neuromodulators in the basal ganglia. Trends Neurosci 13:244–254.

Graybiel AM (1996) Basal ganglia: new therapeutic approaches to Parkinson's disease. Curr Biol 6:368–371.

Graybiel AM (1997) The basal ganglia and cognitive pattern generators. Schizophr Bull 23:459–469.

Graybiel AM, Kimura M (1995) Adaptive neural networks in the basal ganglia. In: Models of information processing in the basal ganglia (Houk JC, Davis JL, Beiser DG, eds), pp 103–116. Cambridge, MA: MIT.

Graybiel AM, Ragsdale Jr CW (1978) Histochemically distinct compartments in the striatum of human, monkey, and cat demonstrated by acetylthiocholinesterase staining. Proc Natl Acad Sci USA 75:5723–5726.

Gsell W, DeSadeleer C, Marchalant Y, MacKenzie ET, Schumann P, Dauphin F (2000) The use of cerebral blood flow as an index of neuronal activity in functional neuroimaging: experimental and pathophysiological considerations. J Chem Neuroanat 20:215–224.

Hevner RF, Liu S, Wong-Riley MT (1995) A metabolic map of cyto-

chrome oxidase in the rat brain: histochemical, densitometric and biochemical studies. Neuroscience 65:313–342.
Hikosaka O (1991) Basal ganglia: possible role in motor coordination and learning. Curr Opin Neurobiol 1:638–643.
Houk JC, Adams JL, Barto AG (1995) A model of how the basal ganglia generate and use neural signals that predict reinforcement. In: Models of information processing in the basal ganglia (Houk JC, Davis JL, Beiser DG, eds), pp 249–270. Cambridge, MA: MIT.
Hubel DH, Wiesel TN, Stryker MP (1978) Anatomical demonstration of orientation columns in macaque monkey. J Comp Neurol 177:361–380.
Jakab R, Hazrati L, Goldman-Rakic P (1996) Distribution and neurochemical character of substance P receptor (SPR)-immunoreactive striatal neurons of the macaque monkey: accumulation SP fibers and SPR neurons and dendrites in "striocapsules" encircling striosomes. J Comp Neurol 369:137–149.
Jiménez-Castellanos J, Graybiel AM (1987) Subdivisions of the dopamine-containing A8–A9-A10 complex identified by their differential mesostriatal innervation of striosomes and extrastriosomal matrix. Neuroscience 23:223–242.
Jiménez-Castellanos J, Graybiel AM (1989) Compartmental origins of striatal efferent projections in the cat. Neuroscience 32:297–321.
Jog M, Kubota Y, Connolly CI, Hillegaart V, Graybiel AM (1999) Building neural representations of habits. Science 286:1745–1749.
Jones EG, Coulter JD, Burton H, Porter R (1977) Cells of origin and terminal distribution of corticostriatal fibers arising in the sensory-motor cortex of monkeys. J Comp Neurol 173:53–80.
Juliano SL, Whitsel BL (1987) A combined 2-deoxyglucose and neurophysiological study of primate somatosensory cortex. J Comp Neurol 263:514–525.
Kawaguchi Y, Wilson CJ, Augood SJ, Emson PC (1995) Striatal interneurons: chemical, physiological and morphological characterization. Trends Neurosci 18:527–535.
Kermadi I, Joseph JP (1995) Activity in the caudate nucleus of monkey during spatial sequencing. J Neurophysiol 74:911–933.
Kimura M (1990) Behaviorally contingent property of movement-related activity in the primate putamen. J Neurophysiol 63:1277–1296.
Kincaid AE, Wilson CJ (1996) Corticostriatal innervation of the patch and matrix in the rat neostriatum. J Comp Neurol 374:578–592.
Koos T, Tepper JM (1999) Inhibitory control of neostriatal projection neurons by GABAergic interneurons. Nat Neurosci 2:467–472.
Künzle H (1977) Projections from the primary somatosensory cortex to basal ganglia and thalamus in the monkey. Exp Brain Res 30:481–492.
Liles SL, Updyke BV (1985) Projection of the digit and wrist area of precentral gyrus to the putamen: relation between topography and physiological properties of neurons in the putamen. Brain Res 339:245–255.
Lindeberg T, Lidberg P, Roland PE (1999) Analysis of brain activation patterns using a 3-D scale-space primal sketch. Hum Brain Mapp 7:166–194.
Malach R, Graybiel AM (1986) Mosaic architecture of the somatic sensory-recipient sector of the cat's striatum. J Neurosci 6:3436–3458.
Mata M, Fink DJ, Gainer H, Smith CB, Davidsen L, Savaki H, Schwartz WJ, Sokoloff L (1980) Activity-dependent energy metabolism in rat posterior pituitary primarily reflects sodium pump activity. J Neurochem 34:213–215.
Mink JW (1996) The basal ganglia: focused selection and inhibition of competing motor programs. Prog Neurobiol 50:381–425.
Moratalla R, Robertson HA, Graybiel AM (1992) Dynamic regulation of *NGFI*-A (*zif*268, *egr*1) gene expression in the striatum. J Neurosci 12:2609–2622.
Nakao Y, Itoh Y, Kuang TY, Cook M, Jehle J, Sokoloff L (2001) Effects of anesthesia on functional activation of cerebral blood flow and metabolism. Proc Natl Acad Sci USA 98:7593–7598.
Parthasarathy HB, Graybiel AM (1997) Cortically driven immediate-early gene expression reflects modular influence of sensorimotor cortex on identified striatal neurons in the squirrel monkey. J Neurosci 17:2477–2491.
Paxinos G, Watson C (1998) The rat brain in stereotaxic coordinates. San Diego: Academic.
Ragsdale Jr CW, Graybiel AM (1990) A simple ordering of neocortical areas established by the compartmental organization of their striatal projections. Proc Natl Acad Sci USA 87:6196–6199.
Ragsdale Jr CW, Graybiel AM (1991) Compartmental organization of the thalamostriatal connection in the cat. J Comp Neurol 311:134–167.
Rolls ET (1994) Neurophysiology and cognitive functions of the striatum. Rev Neurol (Paris) 150:648–660.
Saka E, Elibol B, Erdem S, Dalkara T (1999) Compartmental changes in expression of c-Fos and FosB proteins in intact and dopamine-depleted striatum after chronic apomorphine treatment. Brain Res 825:104–114.
Schultz W, Romo R (1988) Neuronal activity in the monkey striatum during the initiation of movements. Exp Brain Res 71:431–436.
Selemon LD, Goldman-Rakic PS (1985) Longitudinal topography and interdigitation of corticostriatal projections in the rhesus monkey. J Neurosci 5:776–794.
Smith CB (1983) Localization of activity-associated changes in metabolism of the central nervous system with the deoxyglucose method: prospects for cellular resolution. In: current methods in cellular neurobiology (Barker JL, McKelvy JF, eds), pp 269–317. New York: Wiley.
Sokoloff L, Reivich M, Kennedy C, Des Rosiers MH, Patlak CS, Pettigrew KD, Sakurada O, Shinohara M (1977) The [^{14}C]deoxyglucose method for the measurement of local cerebral glucose utilization: theory, procedure, and normal values in the conscious and anesthetized albino rat. J Neurochem 28:897–916.
Swerdlow NR, Koob GF (1987) Dopamine, schizophrenia, mania, and depression: toward a unified hypothesis of cortico-striato-pallido-thalamic function. Behav Brain Sci 10:197–245.
Trytek ES, White IM, Schroeder DM, Heidenreich BA, Rebec GV (1996) Localization of motor- and nonmotor-related neurons within the matrix-striosome organization of rat striatum. Brain Res 707:221–227.
van Vulpen EH, van der Kooy D (1998) Striatal cholinergic interneurons: birthdates predict compartmental localization. Brain Res Dev Brain Res 109:51–58.
Waldvogel HJ, Kubota Y, Fritschy J, Mohler H, Faull RL (1999) Regional and cellular localisation of GABA(A) receptor subunits in the human basal ganglia: an autoradiographic and immunohistochemical study. J Comp Neurol 415:313–340.
White NM, Hiroi N (1998) Preferential localization of self-stimulation sites in striosomes/patches in the rat striatum. Proc Natl Acad Sci USA 95:6486–6491.
Wright AK, Norrie L, Ingham CA, Hutton EA, Arbuthnott GW (1999) Double anterograde tracing of outputs from adjacent "barrel columns" of rat somatosensory cortex. Neostriatal projection patterns and terminal ultrastructure. Neuroscience 88:119–133.
Yarowski L, Kadekaro M, Sokoloff L (1983) Frequency-dependent activation of glucose utilization in the superior cervical ganglion by electrical stimulation of cervical sympathetic trunk. Proc Natl Acad Sci USA 80:4179–4183.